Elaboration and mechanical properties of monolithic and multilayer mullite-alumina based composites devoted to ballistic applications

C. Aharonian, Nicolas Tessier-Doyen, Pierre-Marie Geffroy, Cécile Pagnoux

Elaboration and mechanical properties of monolithic and multilayer mullite-alumina based composites devoted to ballistic applications

C. Aharonian[a,b,c], N. Tessier-Doyen[b,*], P.-M. Geffroy[b], C. Pagnoux[b]

[a] SLFP Bernardaud company, 84 Rue de La lande, F-87520 Oradour sur Glane, France

[b] IRCER, CNRS, Université de Limoges, CEC, 12 rue Atlantis, F-87068 Limoges, France

[c] Bernardaud Company, 27 avenue Albert Thomas F-87100 Limoges France

*Corresponding author at: IRCER, CNRS, Université de Limoges, CEC, 12 rue Atlantis, F-87068 Limoges, France

Tel: +33 587 50 25 00

Fax: +33 587 50 23 01

Email address: nicolas.tessier-doyen@unilim.fr (Nicolas Tessier-Doyen)

Abstract

Both monolithic and multilayer mullite-alumina ceramic composites dedicated to ballistic applications were produced by uni-axial pressing and tape casting before being sintered at 1510°C. The compositions combining andalusite and kaolin in addition to α-alumina exhibit the more promising mechanical properties, reaching the performances of pure ballistic alumina. However, for a given bulk density value, a significant improvement of the performances (Young's modulus and ballistic impedance) only by varying the composition of the monoliths is limited. The second approach reported in this work has consisted in the development of judicious multilayer materials based on the generation of internal residual stresses in thinner layers. Compared to the monolithic materials, the most efficient multilayer configurations exhibit a failure stress improved by +35% and a fracture energy increased by +60%. Indeed, the layers subjected to compressive stress promote a significant crack bifurcation during rupture.

Key words: mullite; multilayer; armour ceramics; mechanical properties; residual stress.

1. Introduction

Modern armor protection systems require more and more lightweight components ensuring sufficient ballistic performances with a low cost of production. In particular, ceramics parts dedicated to armor applications can represent a significant proportion of the overall weight [1-3]. The current available technical ceramics dedicated to armor can be classified in function of the decreasing price/weight indicator: i) hot-pressed boron carbide ceramics exhibiting a low density but a rather great cost of production, ii) silicon carbide materials as intermediate family and iii) alpha alumina-based products belonging to low cost ballistic ceramics group: indeed, regarding carbide-based ceramics, production of such oxide based materials doesn't require expensive processing facilities such as uni-axial/isostatic hot-pressing equipment or carefully controlled atmosphere furnace operating at temperatures up to 1800°C. Conventional industrial processes can therefore be suitable to produce such oxide-based ceramic parts in large series. The significant weight of almost pure alumina materials is today the main drawback, because a density close to 3.9 $g.cm^{-3}$ is restricting for ballistic applications compared to lighter non-oxide based ceramics. However, Medvedovski [2] reported in 2006 the remarkable mechanical performances of alumina/mullite ceramics exhibiting reduced density around 3.5-3.75$g.cm^{-3}$. Hence, developing mullite phase (density ≈ 3.22$g.cm^{-3}$) in such alumina-based materials from extensive and low cost natural raw materials seems to be a promising alternate solution: their decomposition in primary mullite and silica can start at low temperature (typically around 950°C) depending on the type of phyllosilicate, alumina/silica ratio, the particles size and the amount of impurities. For comparison, most of the Al2O3-SiO2 binary systems composed of pure alumina and silica as starting precursors with sufficient proportions of silica promote mullite for significantly greater temperature. In the current study, two families of raw materials can be distinguished: i) hydrated raw materials (generic chemical formula: $2SiO_2 \cdot Al_2O_3 \cdot H_2O$) such as clays and kaolins for example and ii) anhydrous raw materials ($2SiO_2 \cdot Al_2O_3$) belonging to Sillimanite family (such as sillimanite, kyanite and andalusite). Compared to clays and kaolins, kyanite and andalusite exhibit an increase of volume during the decomposition at high temperature which can be of interest in the objective of reducing shrinkage due to sintering. Moreover, the maximum conversion rate into mullite for hydrated raw materials is 64% [4] whereas it reaches 88% for Silimanite group [5]. This residual silica due to the intrinsic decomposition of alumino-silicate raw materials is not favourable for great ballistic performances: indeed, it corresponds to the weakest phase of the materials in terms of mechanical properties. A

solution consists in promoting a dissolution-precipitation reaction between this excess of silica and added α-alumina to form in situ a secondary mullite phase at a higher temperature [6-9].

The main mechanical characteristics required for ballistic ceramics are i) a high surface hardness devoted to damage the penetrator at the impact in order to reduce the penetration depth [10-11] and ii) the ability of the material to absorb energy when cracking [12]. In this way, the approach consisting in shaping multilayer ceramics was proposed by many authors [13-25]: indeed, compared to monolithic materials, inducing internal in-plane compressive residual stresses inside the multilayer structure contributes significantly to improve strength and fracture toughness: as the opposition to crack growth is favoured, the catastrophic failure of the structure is delayed generating a crack shielding. These residual stresses can be generated during the cooling stage of the processing due to a mismatch in the thermal expansion of layers. Moreover, the magnitude of these internal stresses can be varied not only by monitoring the contrast between thermal expansion coefficients but also adjusting individual elastic properties and thickness of each layer.

This article is dedicated to the development of low cost alumina/mullite based materials for ballistic applications using conventional processing facilities currently employed in ceramic industry. The main objective is to promote high stiffness and high fracture strength reducing bulk density close to $3 g.cm^{-3}$. In this way, two approaches are explored:

i) The first approach consists in the elaboration of monolithic ceramics by cold uni-axial pressing of powders. Starting mixtures containing α-alumina combined with kaolin based raw material and/or andalusite in different proportions lead to various alumina/mullite composites after sintering. Considering the conversion rate into mullite of the raw materials, the main objective is i) to promote both primary and secondary mullite phase and ii) to reduce the pore volume fraction and the residual silica phase after sintering. Density, Young's modulus and ballistic impedance are determined for three different families of materials;

ii) The second approach reported in this work is devoted to elaborate multilayer ceramics inducing in-plane compressive thermal stresses at the interface of layers. After a selection of two appropriate alumino-silicate based compositions, the expected additional mechanical performances of such multilayer ceramics

compared to previous monolithic materials are evaluated through 4-point bending tests and Charpy impact test method.

2. Experimental

2.1. Preparation of monolithic materials

Materials are synthetized from initial raw materials: i) P152SB α-alumina (ALTEO company, France, $D_{50} \approx 1.3\mu m$), ii) BIO kaolin as a clay material (supplied by the Kaolins de Beauvoir company, Echassières, France, $D_{50} \approx 2.5\mu m$) composed of 77% of kaolinite, 20% of muscovite and 3% of quartz [26-27] and Kerphalite KA andalusite (Imerys, Glomel, France, $D_{50} \approx 3\mu m$) with quartz (≈1wt.%), alkalis (<0.5wt.%) and hematite (<0.5wt.%) as impurities. Andalusite initially delivered in a batch containing grains with a large particle size distribution (ranging from 0.1 to 5 mm) has been ground during 3h in a dry ball miller. A final screening at 20µm is required to select the smallest particles in order to favour the mullitization reaction at low temperatures [28]. Different stoichiometric mixtures are prepared in such a way that i) a complete decomposition of kaolin or/and andalusite in mullite phase occurs and ii) the residual silica coming from the previous decompositions reacts with an excess of added α-alumina. MgO has been systematically added in slight proportion (1wt%) in order to limit alumina grain growth during the dwell at the maximum temperature [29]. Three main families of compositions have been considered varying the different proportions of starting raw materials added to corundum alumina (Table 1): i) EVO-1 family with both kaolin and andalusite, ii) EVO-2 group containing kaolin without andalusite and iii) EVO-3 compositions exhibiting only andalusite.

Compositions of material	wt.% of starting raw materials			Sintering T (°C)
	α-alumina	kaolin	andalusite	
EVO-1	72-80	10-20	15-25	1550
EVO-2	60-70	20-28	-	1510
EVO-3	47-68	-	32-53	1600

Table 1. Proportion of raw materials in starting compositions and sintering temperatures

Powders have been mixed with water (60wt.%) and a dispersive agent (0.2wt.% in regards with the overall quantity of dried powders, Darvan C) during 4 hours. Then, the suspension has been spray-dried at 180°C to reduce humidity until 3% inside the granules. Green bulk powder compacts have been shaped by uni-axial pressing (60MPa) in respect to the following dimensions: 30mm in diameter and about 8mm in thickness. Sintering treatment has been performed in air (with a maximum temperature of 1510, 1550 or 1600°C during 1h in

function of the considered compositions) in an electric furnace. As the expected complete mullitization for the kaolin raw materials occurs at lower temperature (1350-1450°C) than for andalusite (1600°C), the greater the proportion of added andalusite, the higher the sintering temperature.

2.2. Production of multilayer systems

One typical design chosen for laminar ceramics materials with thermally induced residual stresses is composed of green tapes (thin layers) associated with a powder compact (core) as presented in Figure 1.

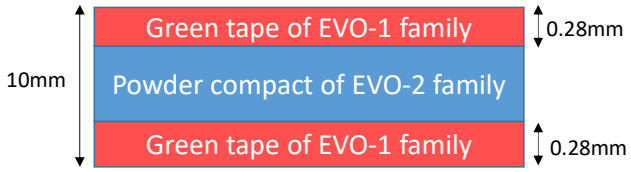

Figure 1: schematic of a multilayer system obtained by uniaxial co-pressing (final dimensions obtained after sintering)

First, thin green tapes are produced by tape casting process, as detailed in previous works [30, 31]. Ceramic suspension is prepared from the EVO-1 powder: an organic solvent (azeotropic solvent: 66% butan-2-one and 34% ethanol), a dispersive agent (phosphate ester, C213, CECA), a binder (polymethacrylate, Degalan 51/70, Degüssa) and a plasticizer (dibutyl phtalate, DPB 400, Sigma Aldrich) are used. The powder is first deagglomerated and dispersed during 1h in the organic solvent with the dispersive agent using ball-milling operating at 210 r.p.m. Then, the binder and the plasticizer are added together and mixed to the slurry in the ball-miller rotating at 120 r.p.m for 12h. The thickness of green tapes obtained by tape casting is about 350 µm after drying.

Second, the multilayer systems are shaped by cold uniaxial pressing under 50 MPa combining i) the powder belonging to EVO-2 group and ii) previous thin green tapes obtained from EVO-1 powder. The pressing die is dedicated to shape plates exhibiting a section of 115×65mm^2 with a thickness of about 13mm. After co-pressing, multilayer sample are debinded (1°C.min^{-1} between 100 and 500°C) and sintered at 1510°C during 1h, with heating and cooling rate of 5°C.min^{-1}.

2.3. Techniques of characterization

After sintering step, microstructure of materials has been observed by Scanning Electron Microscopy. Surface of samples is previously polished (finishing stage of polishing with a 1µm diamond paste). An eventual etching with hydrofluoric acid (10% diluted in water) during 20 seconds can be performed in order to remove amorphous silica phase: this treatment enables to observe the morphology of mullite and alumina phases.

Bulk density (ρ_{bulk}) and pore volume fraction (π) of monolithic materials have been determined using both Archimede's method and helium pycnometer technique.

In order to quantify alumina and mullite phases, X-Ray diffraction technique has been performed with a Brucker-D5000 Siemens equipment in the range 15-120° (gap of 0.012°). Thanks to EVA software, the ratio between integrated intensity of the most intense pics of alumina and mullite (respectively located at 35.14° and 26.27° in the 2θ angle scale) allows to evaluate phase proportions by comparison with a calibration curve obtained previously with perfectly controlled two-phase mixtures.

Ultrasonic pulse echography method in infinite medium has also been employed in reflection configuration to determine room temperature Young's modulus. Operating at a frequency of 10 MHz, longitudinal and transversal waves are generated through the thickness of specimens thanks to emitting/receiving contact transducers. Young's modulus and Poisson's ratio are then calculated from bulk density, longitudinal and transversal ultrasonic velocities [32]. Moreover, pulse echography method in long bar mode has also been used to follow in situ Young's modulus variation of a sintered monolithic material in order to determine accurately the temperature corresponding to the formation of viscous phase.

Dilatometric measurements have been performed with green samples ($5x5x20mm^3$) in order to determine the coefficient of thermal expansion on the cooling step (corresponding typically to the slope of the curve on a given range of temperature).

4-point bending tests have been carried out with a universal testing machine (Instron 5969) operating at a speed of $0.5mm.min^{-1}$ with a loading sensor of 20kN. After a previous machining of bar-type specimens ($80\times10\times10mm^3$), the static mechanical performance of monolithic and multilayer ceramic materials has been evaluated through the facture stress value. The test has been performed using systematically 5 samples per system.

Finally, Charpy impact testing method (pendulum CEAST 6545/1000 with a maximum energy of 25J) has been used to compare the fracture energy performances of the different

materials. 5 samples have been investigated for each material to report an average value in the section of results. Square section specimens ($55\times10\times10mm^3$) exhibiting a V-notch of 2mm in depth have been specifically prepared with a diamond-coated saw. The amount of energy absorbed during fracture has been determined both from initial and final heights of the hammer and the broken section of the sample ($80mm^2$) in order to be normalized (E_{Abs} has been expressed in $J.m^{-2}$).

3. Results and discussion

3.1. Microstructure, density and quantification of phases

After polishing, figures 2 a), b) and c) show the microstructure of EVO-1, EVO-2 and EVO-3 materials respectively. Quantity and size of pores seem to be greater for EVO-3 materials compared to EVO-1 and EVO-2 families.

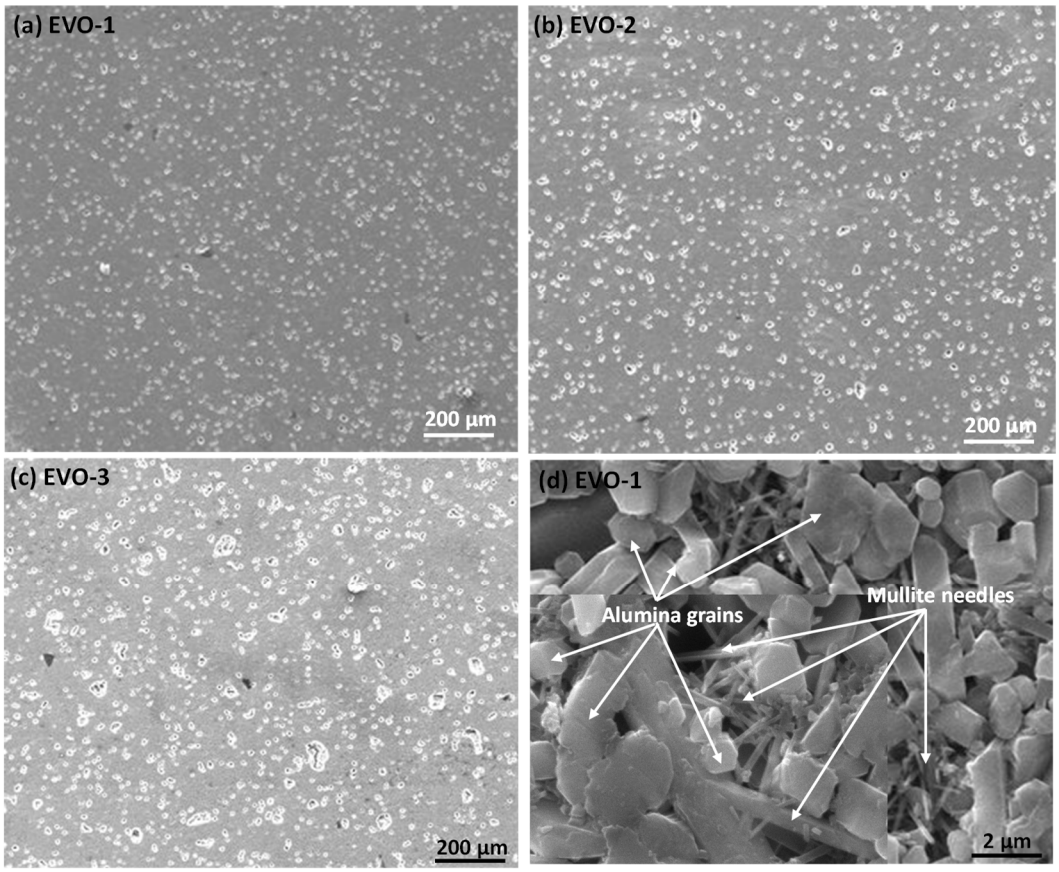

Figure 2. Microstructure of a) EVO-1, b) EVO-2, c) EVO-3 materials and d) Typical morphology of alumina and mullite phases in EVO-1 materials after chemical etching with hydrofluoric acid

An observation carried out with at a higher magnification (Figure 2 d) shows EVO-1 microstructure after an etching with hydrofluoric acid: a large network of entangled mullite needles is clearly visible whose average diameter ranges from 0.4 to 3µm. Some coarse mullite grains, whose remarkable length can exceed 10µm, correspond probably to secondary mullite, as primary mullite coming from the decomposition of kaolinite or andalusite remains generally smaller [33]. From these observations, associating both kaolin and andalusite in the mixture instead of adding kaolin and andalusite separately seems to give denser final microstructures with finer pores in limited proportion.

Pore volume fraction (π), bulk density (ρ_{bulk}) and weight proportions of residual alumina and formed mullite phases after sintering for the three studied families of monolithic materials are reported in Table 2.

Monolithic materials	π	ρ_{bulk} (g/cm^3)	wt.% of phases	
			α-alumina	mullite
EVO-1	3-8%	3.22-3.61	45-66	40-58
EVO-2	4-12%	2.83-3.44	41-49	35-52
EVO-3	6-24%	2.46-3.28	28-55	50-74

Table 2. Bulk density, pore volume fraction and proportions of α-alumina and mullite after sintering

Density measurements obtained by Archimedes' method confirm that pore volume fraction remains almost constant for the two first groups whereas it is slightly greater for the materials with only andalusite addition (EVO-3). Moreover, from general point of view, EVO-3 materials exhibit a lower density after sintering at rather high temperature (1600°C) in comparison with the families containing kaolinite material precursor (EVO-1 and EVO-2 compositions) after a lower heat treatment at 1550 or 1510°C, respectively. This low bulk density is probably not only due to the formation of significant amount of mullite (systematically greater than 50wt.%) which decreases the intrinsic density of the solid part but also to the too high pore volume fraction. In addition, considering that the decomposition of andalusite leads to a fine interconnected mullite network in which silica is trapped, the reaction with the added alumina in excess to form mullite is not favoured for EVO-3 compositions. On the contrary, it can be expected that the main proportion of this silica has reacted with alumina to form secondary mullite phase in the case of EVO-1 and EVO-2 materials. Finally, results of Table 2 seem to highlight that the pore and bulk density values may be more related to bulk compositions rather than the precursor's kind of mixture because an overlapping of values can be observed for the 3 different families of materials.

3.2. Young's modulus and ballistic impedance of monolithic materials

In addition to Young's modulus and bulk density, a criteria to evaluate ballistic performances of a given ceramic material is ballistic impedance (I), as defined in the equation 1 [1].

$$\mathbf{I} = \sqrt{\rho_{\mathbf{bulk}} \times \mathbf{E}} \qquad \text{eq. 1}$$

Figure 3 shows the variation of experimental Young's modulus and ballistic impedance values in function of bulk density.

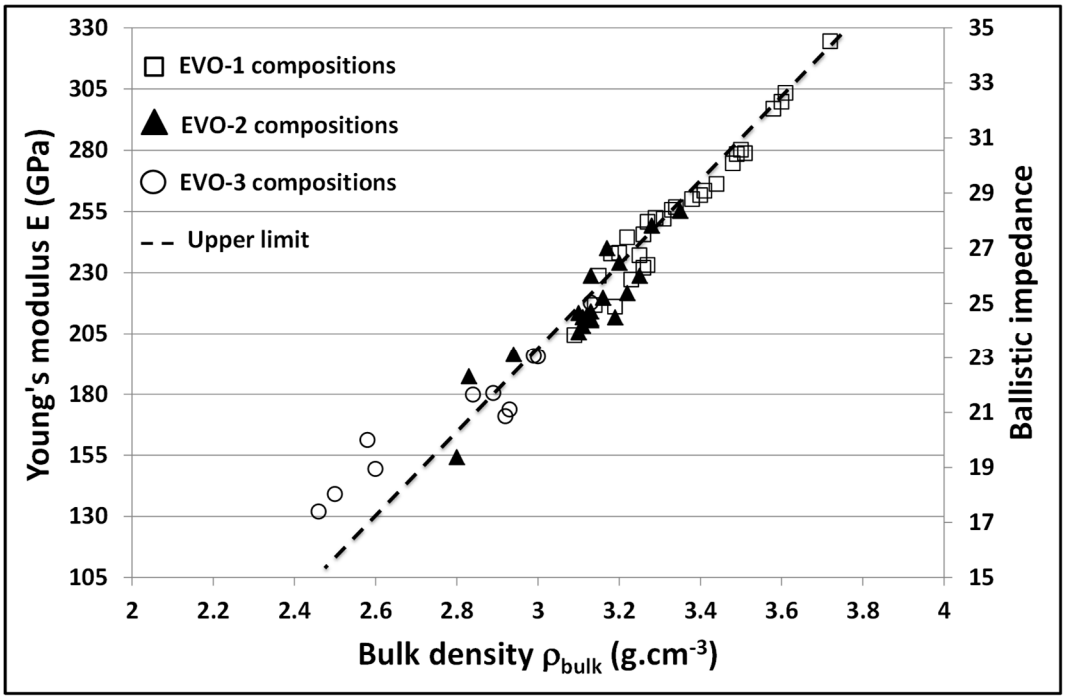

Figure 3. Young's modulus and ballistic impedance vs bulk density for monolithic alumino-silicate based materials (EVO-1, EVO-2 and EVO-3 compositions)

The experimental values reported in figure 3 follow an almost linear evolution, regardless of the alumina/mullite proportion in the composition of final monolithic materials. The Young's modulus (E) is then almost proportional to the density so as to the ballistic impedance. EVO-1 materials family presenting in general the richest compositions in α-alumina exhibits the greater performances. In comparison, commercial ballistic alumina impedance ranges from 35 to 38 [34]. However, lightweight monolithic alumino-silicate materials (EVO-3 type) present the weakest ballistic performances which is in agreement with data reported in Table 2: specimens belonging to this family exhibit the lowest density values due to i) mainly a greatest pore volume fraction and, ii) to a lesser extent, a higher proportion of mullite phase (true density close to 3.22g.cm^{-3} compared to 3.9g.cm^{-3} for pure alumina). Considering the

chosen sintering conditions which have been optimized in the best possible way for the 3 compositions, these results suggest that ballistic impedance of monolithic alumino-silicate materials cannot overcome the upper limit indicated.

The solution suggested in this work to improve the mechanical performances of alumino-silicate materials is to combine different compositions through multilayer structures. Typically, an ideal system combines a high surface stiffness (Young's modulus), a density value and sintering temperature as low as possible. The expected enhancing of mechanical performances can be induced by a compressive surface stress developed during the cooling step of the sintering.

3.3. Concept of multilayer materials and individual properties of layers

The in-plane residual compressive surface stress in the material is induced by multilayer design based on two materials noted A and B with different thermal expansion coefficient and Young's modulus noted α_a, α_b and E_a, E_b respectively (figure 4). R. Bermejo et al. [35] have highlighted the significant improvement of mechanical properties exhibited by such multilayer structure with residual compressive internal stresses in regards with monolithic materials.

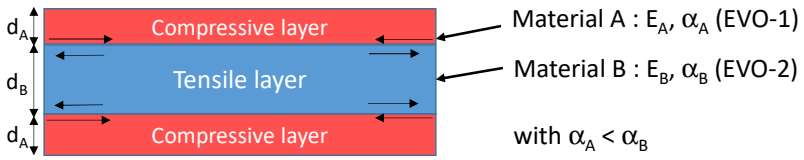

Figure 4. Concept of compressive thin layers induced by thermal stresses during the cooling in a symmetric tri-layer system

The residual compressive stresses generated in the outer layers A (σ_A) and the tensile stress in the thick layer B (σ_B) can be estimated using equations 2 and 3, as following [36-37]:

$$\sigma_A = -\frac{E_A . E_B . d_B . (\alpha_B - \alpha_A) . \Delta T}{(1-\upsilon) . (2 . E_A . d_A + E_B . d_B)} \qquad \text{eq.2}$$

$$\sigma_B = \frac{2 . E_A . E_B . d_A . (\alpha_B - \alpha_A) . \Delta T}{(1-\upsilon) . (2 . E_A . d_A + E_B . d_B)} \qquad \text{eq.3}$$

ν corresponding to the Poisson's ratio assumed to be identical for each material A and B, d_A and d_B are the thicknesses of each layer A and B, respectively. $\Delta T = (T_{free} - T_{amb})$ is the difference between the temperature from which the stresses are completely relaxed noted T_{free} (unconstrained multilayer system) and the room temperature (T_{amb}) on the cooling stage of sintering. The free of stress temperature T_{free} has been estimated from the Young's modulus variation versus the temperature thanks to pulse echography method operating in long bar mode.

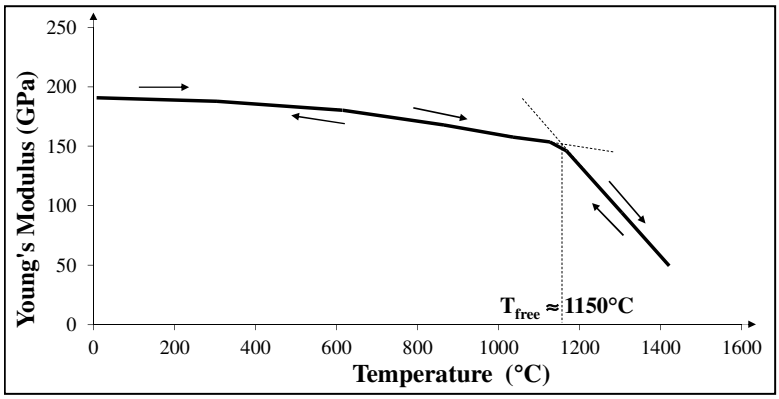

Figure 5: Typical evolution of Young's modulus versus the temperature of a monolithic specimen (EVO-2 family) previously sintered at 1510°C to determine T_{free} value

Figure 5 shows the reversible evolution of Young's modulus versus the temperature of a previously sintered monolithic specimen at 1510°C belonging to EVO-2 materials. A slight decrease of about 35 GPa between room temperature and 1150°C is observed due to thermal expansion of the specimen: indeed, the weakening of interatomic bonds occurring when the temperature increases is responsible for the reduction of both bulk density and velocity of ultrasonic waves. Above 1150°C, the Young's modulus is significantly affected highlighting the formation of viscous flux promoted by residual silica phase inside the material (as explained previously to describe Figure 2). So it is assumed that during the cooling stage after the co-sintering of multilayered materials, the magnitude of internal thermal stresses starts when the temperature (T_{free}) is below 1150°C.

The main properties (density, Young's modulus Poisson's ratio, coefficient of thermal expansion between 1150 and 20°C, flexural strength and absorbed energy determined through Charpy impact testing method) of EVO-1 and EVO-2 materials chosen to be combined to perform multilayer structures are reported in Table 3.

Material	Al_2O_3 wt.%	ρ_{bulk} (g/cm^3)	E (GPa)	ν	$\alpha_{[1150\text{-}20°C]}$ (°C^{-1})	$\sigma_{R[4pts]}$ (MPa)	E_{Abs} (J.m^{-2})
EVO-1	72%	≈3.37	255±2	0.24±0.01	≈6.2×10^{-6}	160±8	20±1
EVO-2	66%	≈3.20	190±2	0.24±0.01	≈8.6×10^{-6}	140±7	20±1

Table 3. Characteristics of monolithic materials chosen for multilayer structures

The thermal expansion coefficients values (α) corresponds to the average slope of dilatometric curve during the cooling in the range 1150°C-20°C. To define an optimal design of multilayers from the evaluation of internal stresses, EVO-1 has been chosen as the layer to be in a compressive state after cooling: indeed, a higher thermal expansion coefficient of EVO-2 (8.6×10^{-6}°C^{-1} against 6.2×10^{-6}°C^{-1} for EVO-1) imposes at room temperature a higher contraction to EVO-1 than expected. The thickness of each layer has to be adjusted in such manner that the magnitude is sufficiently high to induce the higher compressive stress (equations 2 and 3) preventing the structure from breaking: the magnitude of induced internal stresses has to be lower than 4-point flexural stress values of each separate monolithic material. Fracture energy evaluated from Charpy test shows similar values from each EVO-1 and EVO-2 individual materials.

3.4. Mechanical properties of multilayer systems with residual internal stresses

Three different systems of multilayer materials have been studied (Figure 6): i) system I in which two thin compressive layers cover both sides of the thick powder compact, ii) system II with just one compressive layer in the center on the sample and iii) system III exhibiting three compressive layers (two on each side and one located in the middle). For each design, the co-sintering temperature is 1510°C during 1h.

	I	II	III
Multilayer design			
$\sigma_{R[4pt]}$ (MPa)	217±7 (+35%)	187±5 (+25%)	161±6 (+1%)
E_{Abs} (J.m^{-2})	37±1 (+46%)	51±1 (+60%)	29±2 (+31%)

Figure 6. Design of three chosen multilayer systems and mechanical properties compared to EVO-1 monolithic materials taken as a reference (the increase is expressed in % in brackets)

Each system is symmetric in such a way that the final thickness of thin compressive layers is $d_A \approx 280$ µm whereas the thickness of the thick tensile layers is $d_B \approx 9.5$ mm (system I) or $d_B \approx 5$ mm (systems II and III). As a consequence, the overall thickness of the final fired multilayer specimen is ≈ 10 mm. Due to symmetry, the in-plane shrinkage is homogeneous during sintering. Figure 7 a) shows the interface between EVO-1 tape and EVO-2 core: after

sintering, a good interfacial adhesion (no visible delamination) between the two layers can be observed. On the basis of equations 2 and 3 and depending on the considered system, the magnitude of compressive and tensile internal stress has been estimated to range from -593 to -632 MPa in the thin layers and from +37 to +66MPa in the thick layers, respectively.

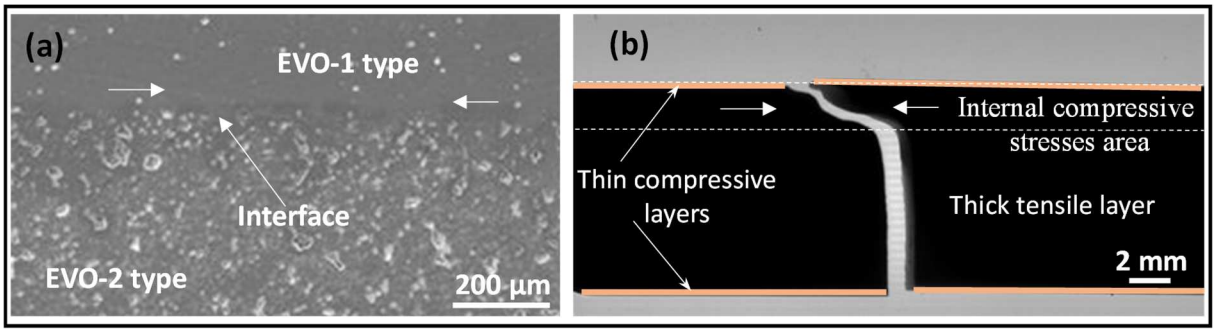

Figure 7. a) SEM micrograph of the interface in multilayer system before failure and b) path deviation of the crack (system I) after failure obtained by 4-point bending test

From general point of view, values reported in Figure 6 shows that the maximum flexural strength ($\sigma_{R[4pt]}$) and the absorbed energy obtained by Charpy tests (E_{Abs}) for all systems are greater than EVO-1 individual properties. The highest stress to rupture value is obtained with the system I compared to the system III which does not exhibit a significant improve in the failure stress. This can be explained by unexpected interactions between developed stresses in the compressive-tensile layers (as the thickness of EVO-2 layer is reduced compared to system I) and/or a weakening of interfacial adhesion limiting the magnitude of compressive stresses in the thinner layers. However, an increase of energy of rupture (+35%) is observed for this system III, but systems I and II exhibit a further improvement of absorbed energy which is undoubtedly due to the effect of compressive layers (values of E_{Abs} are multiplied by 2 approximately).

The picture of Figure 7 b) shows the effect of the compressive stresses on the crack deflection in multilayer system I (observation of the post-mortem specimen subjected to 4-point bending test thanks to optical backlight with a light table): i) after initiation, the crack seems to propagate freely and vertically in the thickness of the tensile layer assuming that this is due to the uniformity of imposed external stress; ii) from these observations, it can be deduced that a first deflection of the crack path occurs very early, at a distance up to 2 mm from the top of the specimen, and that a second deflection seems to happen closer to the upper layer (at a distance of about 600 µm from the top surface of the specimen, corresponding to

about twice or 3 times the thickness of the upper layer). From these pots-mortem observations and taking into account that the compressive stress in the lower layer is supposed to contribute to delay the initiation of the crack compared to unconstrained monolithic materials, it can be assumed that delocalized internal compressive stresses in the thicker layer oppose to the crack propagation in two times, which contributes to increase the overall energy rupture of such multilayer materials.

4. Conclusions

Monolithic and multilayer alumino-silicate composite ceramic materials dedicated to ballistic applications have been fabricated from the synthesis of low cost natural raw materials mixtures (α-alumina, kaolin and andalusite). In the first approach concerning monoliths, the main objective was to prepare by uni-axial pressing sintered alumina/mullite materials with both great ballistic impedance/Young's modulus and reduced bulk density (around 3g.cm^{-3}). The family of compositions combining andalusite and kaolin (EVO-1) exhibit the more promising mechanical properties converging towards the performances of pure ballistic α-alumina. Whatever the composition, it has been highlighted that Young's modulus and ballistic impedance evolve linearly with the bulk density of materials. Even if the chosen sintering conditions have been optimized in the best possible way for the 3 compositions, these results suggest that mechanical performances of monolithic alumino-silicate materials cannot overcome an upper limit.

In order to improve mechanical properties, an alternate approach has secondly consisted in inducing in-plane residual compressive stress in multilayer system on the basis of previous monoliths whose thermal expansion mismatch, elastic properties and the thickness of each layer have been carefully monitored. Three different systems consisting of thin tapes (280µm) combined with compacts have been co-pressed and co-sintered to induce after cooling compressive stresses. Compared to the individual monoliths, the most promising configurations exhibit a fracture stress evaluated by 4-point bending test improved by +35% and a fracture energy value multiplied by more than two (+60%). The effect of crack bifurcation directly involved by the thin compressive layer which is both responsible for an improvement of stress to rupture and energy absorption has been highlighted after failure of specimens. To pursue within this work, it could be interesting to perform ballistic tests in real conditions on such constrained mullite/alumina multilayer composites materials.

References

[1] E. Medvedovski, Alumina Ceramics for Ballistic Protection, Am. Ceram. Soc. Bull. 81 (2002) 45-50.

[2] E. Medvedovski, Alumina-Mullite Ceramics for Structural Applications, Ceram. Int. 32 (2006) 369-375.

[3] E. Medvedovski, Ballistic performance of armour ceramics: influence of design and structure - Part 1, Ceram. Int. 36 (2010) 2103–2115.

[4] F. Mazel, M. Gonon, G. Fantozzi, Manufacture of mulita substrates from andalusite for the development of thin solar cells, J. Eur. Ceram. Soc. 22 (2002) 453-461.

[5] E.T. Goergen, D.L. Whitney, M.E. Zimmermann, T. Higara, Deformation-induced polymorphism transformation experimental deformation of kyanite, andalusite and sillimanite, Tectonophysics 454 (2008) 23-25.

[6] K.-C Liu, G. Thomas, A. Caballero, J.S. Moya, S. de Aza, Mullite formation in kaolinite-α-alumina, Acta Metall. Mater. 42 (1994) 489-495.

[7] P. Dubreuil, V. M. Sobolev, Andalusite: a promising material for manufacturing high-quality refractories, Refract. Ind. Ceram. 40 (1999) 152-158.

[8] H.J. Kleebe, F. Siegelin, T. Straubinger, G. Ziegler, Conversion of Al2O3-SiO2 powder mixtures to 3:2 mullite following the stable or metastable phase diagram, J. Eur. Ceram. Soc. 21 (2001) 2521, 2533.

[9] J. Aguilar-Santillan, H. Balmori-Ramirez, R.C. Bradt, Processing Research Dense Mullite from Attrition milled Kyanite and α-Alumina, J. Ceram. Process. Res. 8 (2007) 1-11.

[10] C. Aharonian, P.-M. Geffroy, N. Tessier-Doyen, C. Pagnoux, New elaboration route of oxycarbide SiC/B4C composite layers for ballistic applications, J. Sol-Gel Sci. Tech. 80 (2017) 626-634.

[11] E. Lach, Mechanical Behaviour of Ceramics and their Ballistic Properties, Ceram. Forum. Inter. 70 (1993) 486-490.

[12] D.J. Viechnicki, M.J. Slavin, M.I. Kliman, Development and Current Status of Armor Ceramics, Ceram. Bull. 70 (1991) 1035-1039.

[13] T. Chartier, D. Merle, J.L. Besson, Laminar Ceramic Composites, J. Eur. Ceram. Soc. 15 (1995) 101-107

[14] D.J. Green, P. Cai, G.L. Messing, Residual stresses in alumina-zirconia laminates, J. Eur. Ceram. Soc. 19 (1999) 2511-2517

[15] M.P. Rao, A.J. Sánchez-Herencia, G.E. Beltz, R.M. McMeeking, F.F. Lange, Laminar Ceramics that Exhibit a Threshold Strength, Science 286 (1999) 102-105.

[16] B.F. Sørensen, Thermally Induced Delamination of Symmetrically Graded Multilayers, J. Am. Ceram. Soc. 85 (2002) 858-864.

[17] R. Bermejo, Y. Torres, A.J. Sánchez-Herencia, C. Baudin, M. Anglada, L. Llanes, Residual Stresses, Strength and Toughness of Laminates with Different Layer Thickness Ratios, Acta Mater. 54 (2006) 4745-4757.

[18] M.U. Übeyli, R.O. Yildirimb, B. Ögel, Investigation on the ballistic behavior of Al2O3/Al2024 laminated composites, J. Mater. Proc. Tech. 196 (2008) 356-364.

[19] R. Bermejo, J. Pascual, T. Lube, R. Danzer, Optimal Strength and Toughness of Al2O3-ZrO2 Laminates designed with External and Internal Compressive Layers, J. Eur. Ceram. Soc. 28 (2008) 1575-1583.

[20] L. Sestakova, R. Bermejo, Z. Chlup, R Danzer, Strategies for fracture toughness, strength and reliability optimisation of ceramic-ceramic laminates, Int. J. Mat. Res. 102 (2011) 1-14.

[21] B.F. Sørensen, H. Toftegaard, S. Linderoth, M. Lundberg, S. Feih, Strength and Failure modes of Ceramics Multilayers, J. Eur. Ceram. Soc. 32 (2012) 4165-4176.

[22] R. Pavlacka, R. Bermejo, Y. Chang, D.J. Green, G.L. Messing, Fracture Behavior of Layered Alumina Microstructural Composites with Highly Textured Layers, J. Am. Ceram. Soc. 96 (2013) 1577-1585.

[23] K. Boussois, N. Tessier-Doyen, P. Blanchart, High-Toughness Silicate Ceramic, J. Eur. Ceram. Soc. 34 (2014) 119-126.

[24] K. Boussois, S. Deniel, N. Tessier-Doyen, D. Chateigner, C Dublanche-Tixier, P. Blanchart, Characterization of Textured Ceramics containing Mullite from Phyllosilicates, Ceram. Inter. 39 (2013) 5327-5333.

[25] C.-Y. Huang, Y.-L. Chen, Design and impact resistant analysis of functionally graded Al2O3–ZrO2 ceramic composite, Mater. Design 91 (2016) 294-305.

[26] J. Bourret, N. Tessier-Doyen, B. Naït-Ali, F. Pennec, A. Alzina, C.S. Peyratout, D.S. Smith, Effect of the Pore Volume Fraction on the Thermal Conductivity and Mechanical Properties of Kaolin-Based Foams, J. Eur. Ceram. Soc. 33 (2013) 1487-1494.

[27] O. Castelein, B. Soulestin, J.P. Bonnet, P. Blanchart, The influence of heating rate on the thermal behaviour and mullite formation from a kaolin raw material, Ceram. Inter. 27 (2001), 517-522.

[28] M.L. Bouchetou, J.P. Ildefonse, J. Poirier, P. Daniellou, Mullite grown from fired andalusite grains: the role of impurities and of the high temperature liquid phase on the kinetics of mullitization and consequences on thermal shocks resistance, Ceram. Inter. 31 (2005) 999-1005.

[29] S. Lahiri, S. Sinhamahapatra, H. Sekhar Tripathi, K. Dana, Rationalizing the role of magnesia and titania on sintering of α-alumina, Ceram. Inter. 42 (2016) 15 405-15 413

[30] P.-M. Geffroy, T. Chartier, J.F. Silvain, Preparation by tape casting and hot pressing of copper carbon composites films, J. Eur. Ceram. Soc. 27 (2007) 291-299.

[31] P.-M. Geffroy, A. Vivet, L. Nguyen, E. Blond, N. Richet, T. Chartier, Elaboration of $La_{1-x}Sr_xFe_{1-y}Ga_yO_{3-\delta}$ multilayer membranes by tape casting and co-firing for syngas application, J. Eur. Ceram. Soc. 33 (2013) 1849–1858.

[32] N. Tessier-Doyen, J.-C. Glandus, M. Huger, Experimental and 2D-Numerical Study of Elastic Behaviour of Heterogeneous Model Materials with Spherical Inclusions, J. Mater. Sci. 42 (2007) 5826-5834.

[33] M.A. Sainz, F.J. Serrano, J.M. Bastida, A. Caballero, XRD microstructural analysis of mullites obtained from kaolinite-alumina mixtures, J. Eur. Ceram. Soc. 20 (2000) 403-412.

[34] C. Aharonian, Elaboration de matériaux céramiques composites et/ou d'architectures lamellaires pour la protection balistique des personnes et des matériels, PhD thesis, SLFP-Bernardaud company - Limoges University (2014) 164 p.

[35] R. Bermejo, J. Pascual, T. Lube, R. Danzer, Optimal strength and toughness of Al2O3-ZrO2 laminates designed with external and internal compressive layers, J. Eur. Ceram. Soc. 28 (2008) 1575-1583.

[36] R. Bermejo, C. Baudin, C. Moreno, L. Llanes, A.J. Sánchez-Herencia, Processing Optimisation and Fracture Behaviour of Layered Ceramic Composites with Highly Compressive Layers, Comp. Sci. Tech. 67 (2007) 1930-1938.

[37] A.V. Virkar, J.L. Huang, R.A. Cutler, Strengthening of Oxide Ceramics by Transformation-Induced Stresses, J. Am. Ceram. Soc. 70 (1987) 164-170.

Acknowledgments

Authors would like to thank the French General Direction of Army (DGA) for the financial support devoted to “Brennus” national research project.